Insights on hexagonal TbMnO3 for optoelectronic applications: From powders to thin films

Thomas Fix, Guy Schmerber, Jean Luc Rehspringer, Mircea Rastei, Stéphane Roques, Jeremy Bartringer, Abdelilah Slaoui

Insights on hexagonal $TbMnO_3$ for optoelectronic applications: from powders to thin films

T. Fix[1*], G. Schmerber[2], J.-L. Rehspringer[2], M. V. Rastei[2], S. Roques[1], J. Bartringer[1], A. Slaoui[1]

[1] ICube laboratory, CNRS and Université de Strasbourg, 23 rue du Loess, 67037 Strasbourg, France

[2] Institut de Physique et Chimie des Matériaux de Strasbourg, CNRS and Université de Strasbourg, 23 rue du Loess, 67034 Strasbourg, France

* Corresponding author. Tel.: +33 388106334, Fax +33 388106548. E-mail address: tfix@unistra.fr

Abstract

In this work, we first report on the fabrication of $TbMnO_3$ (TMO) powders and doping with In, Lu, Gd, Sm, Nd, Y. In and Nd atoms were found to significantly reduce the cell size while preserving an orthorhombic structure. Conversely, we show that hexagonal h-TMO, indium doped TMO (h-In-TMO), yttrium doped TMO (h-Y-TMO), and $YMnO_3$ (h-YMO) can be obtained epitaxially using pulsed laser deposition (PLD) on Pt (111) // Al_2O_3 (0001). The evolution of the optical properties was measured for the PLD films and a direct bandgap of 1.5-1.6 eV was found for h-TMO and doped h-TMO films. The h-TMO, h-In-TMO and h-Y-TMO showed no sign of ferroelectricity at room temperature as opposed to h-YMO. No short-circuit current in solar cell configuration was found under 1 sun illumination. However a photovoltaic behaviour was observed by surface photovoltage for the h-Y-TMO and h-YMO, indicating that Y incorporation in h-TMO is helpful for the photovoltaic properties.

Keywords: thin films; oxide materials; photoconductivity and photovoltaics

1. Introduction

Ferroelectric photovoltaics (FPV) are different from conventional *pn* junction solar cells because the photogenerated electron hole pairs are separated by the ferroelectric polarization originating from the polar noncentrosymmetry of the structure. This can lead to open circuit voltage values (V_{oc}) much higher than the bandgap of the materials[1] and to the possibility of switching the direction of the photocurrent by applying an electric field pulse to the device[2]. The main limitation of ferroelectric photovoltaics has been the high bandgap of such ferroelectric materials. A prototypical example is $BiFeO_3$ with a bandgap up to 2.7 eV[3, 4]. A solution was provided by considering a double perovskite Bi_2FeCrO_6 (BFCO) in which the bandgap could be reduced from 2.6 to 1.9 eV[2, 5, 6] simply by controlling the Fe/Cr order. Along the same line, other materials are being investigated such a $KBiFe_2O_5$ (with a bandgap ranging between 1.6-2.3 eV)[7]. Still, the efficiency record of FPV solar cells remains with BFCO with a power conversion efficiency of 8.1 %[2]. This value corresponds to the efficiency record of oxide based solar cells, shared with Cu_2O[8, 9].

In a previous study by Han et al., hexagonal manganite thin films were proposed as a ferroelectric solar cell absorber, namely h-$LuMnO_3$ and h-$YMnO_{3[10]}$. It was found that the photocurrent was reversibly switchable, with an open circuit voltage V_{oc} up to 0.71 V and a short circuit current density J_{sc} up to 0.55 mA/cm², leading to a maximum conversion efficiency of around 0.1 %[10]. The latter value was two orders of magnitude higher than a similar study with h-$TmFeO_3$ and h-$LuFeO_3$ absorbers[11].

In this work, inspired by a theoretical article by Y. Tsymbal et al.[12], we focus on hexagonal rare-earth manganites (h-$RMnO_3$ where R is a rare earth ion), and in particular on h-$TbMnO_3$ (h-TMO). These materials have received a lot of interest due to their improper structural ferroelectricity and multiferroic properties, that differ from the orthorhombic TMO (o-TMO) phase. o-TMO is indeed a spin-driven ferroelectric perovskite[13-16] and it was proposed as an ultraviolet photodetector[17]. In h-TMO ferroelectricity originates from the rotation and tilt of the MnO_5 polyhedra[18]. Orthorhombic rare-earth manganites such as o-TMO display ferroelectric ordering at low temperature, below 100 K (41 K for o-TMO films)[15]. The orthorhombic phases are generally obtained in the bulk when the rare-earth radius is large (R = La, Pr, Nd, Sm, Eu, Gd, Tb, Dy). In contrast, for smaller radius (R = Y, Ho, Er, Yb, Lu) the hexagonal structure is obtained and ferroelectricity can reach 600-1000 K[18]. However the h-TMO (R = Tb) phase can be grown even if unfavourable thanks to the concept of epitaxial stabilisation using appropriate substrate such as yttria-stabilized zirconia (YSZ) (111) [19] or buffer layers such as Pt(111)//Al_2O_3 (0001)[18, 20]. The growth of this material is complex due to the fact that the orthorhombic phase of TMO is more favourable and generally obtained. However the h-TMO material has been shown with a large remnant ferroelectric polarization (8 μC/cm²) at room temperature,

making it a potential candidate for FPV[18]. In addition, h-TMO offers a direct bandgap of about 1.4 eV [12], which is almost the ideal value for a single bandgap photovoltaic absorber, together with an absorption coefficient (for polarization perpendicular to the *c* direction) almost two times larger than CdTe in the visible[12]. For a h-TMO thickness of 0.5 µm, the maximum photovoltaic energy conversion efficiency was calculated to be 32 %, compared to 27 % for CdTe and 2 % for $BaTiO_{3[12]}$. These predictions are very promising and the aim of the current work is to confront these calculations to experiments.

In the present work we first provide a simple guide on the deposition of h-TMO by pulsed laser deposition (PLD). A systematic investigation of doping effects of TMO powders and films by different elements such as In, Lu, Gd, Sm, Nd, Y, is presented. We also describe the potential of h-TMO as a photovoltaic absorber, by demonstrating significant values of surface photovoltage effects.

2. Experimental procedure

The TMO and doped TMO powders were prepared as follows. For pure TMO, first Tb_2O_3 powders (8.070 g) were poured in nitric acid (~50 ml) and heated, while stirring with a magnetic bar until a colourless solution was obtained. Then, manganese (II) acetate tetrahydrate (10.812 g) was poured in deionized water (~100 ml). The two solutions were poured into one beaker. Citric acid (15.4 g) is dissolved in the solution together with ethylene glycol (5 g, using the Pecchini method). The excess of water is evaporated and a viscous liquid without precipitate appears. This compound is pre-calcinated in a furnace at 350 °C for two hours, mechanically ground in a mortar, and further calcinated at 750 °C for 1 h in air. The obtained powder is ground again, pressed into a pellet and sintered at 850°C for 1 h in air. For the doped TMO powders, the dopants were introduced in the required quantities in the manganese (II) acetate tetrahydrate solution in the form of lutetium (III) nitrate hydrate, gadolinium (III) nitrate hexahydrate, samarium (III) nitrate hexahydrate, neodymium (III) nitrate hexahydrate, and yttrium (III) nitrate hexahydrate, respectively. For indium doping, the required In metal quantity was poured in nitric acid and heated at 60 °C for one hour until disappearance of the metal. The solution was then poured into the solution of the manganese (II) acetate tetrahydrate. The pictures of the powders are shown in the supplementary information (SI, Figure S1).

The substrates used for deposition were Al_2O_3 (0001) one side polished (ALO) (insulating, thickness 0.5 mm). A 4-6 nm thick Pt layer was deposited at 450 °C in high vacuum on ALO (0001). The PLD process was performed using a KrF laser (248 nm), for the Pt target with a 10 Hz repetition rate and a laser fluence of around 5-6 J/cm² ; for the TMO targets with a 4-10 Hz repetition rate and a laser fluence of

around 1-2 J/cm^2. The deposition of h-TMO was carried out at 750 °C under an oxygen pressure of 10^{-2} mbar. h-TMO film thicknesses were in the 40-52 nm range. The as-grown films were cooled down under the same atmosphere at a rate of 10°C/min until 300°C, below this temperature it was naturally cooled down until room temperature. Around 30 samples were deposited for the study. The pictures of the films are shown in the supplementary information (SI, Figure S1).For the fabrication of solar cells, a mask was placed on the h-TMO films with openings of 1 mm². Indium tin oxide (ITO) was deposited by PLD through the mask at 250 °C in 10^{-2} mbar O_2.

Doped TMO powders were investigated with a Bruker-AXS D8 Advance X-ray diffractometer with Cu $K_{\alpha 1}$ radiation (40 kV, 40 mA, 0.154056 nm). Lattice parameters of the powders were refined using the FullProf Suite. The crystalline structure of the TMO films was analyzed by X-ray diffraction using a Rigaku SmartLab diffractometer equipped with a monochromatic source delivering a Cu $K_{\alpha 1}$ incident beam (45 kV, 200 mA, 0.154056 nm). X-ray θ−2θ and reflectivity were performed in order to look for the film structure, check the presence of spurious phases, and determine the Pt film thickness (see SI Figure S2). Scanning electron microscopy (SEM) was performed with a Gemini 500-ZEISS apparatus and the stoichiometry was checked by Energy-dispersive X-ray spectroscopy (EDS) (see SI Figure S3). The optical properties of the undoped and doped h-TMO films were investigated by spectroscopic ellipsometry using a HORIBA Uvisel Lt M200 FGMS (210–880 nm) apparatus. An anisotropic uniaxial layer was inserted on top of the Pt//Al_2O_3 structure to simulate the undoped and doped h-TMO films. The birefringence of the films had to be considered in the models. The dispersion formula for both the ordinary (o) and extraordinary (e) components were based on the Adachi-New Forouhi model[21]. The goodness-of-fit values (Chi Square χ^2) were always better than 0.25. The spectroscopic ellipsometry analysis was also used to determine the TMO films thicknesses (see SI Figure S4). The ferroelectric properties were investigated by the Piezoresponse Force Microscopy (PFM) technique using an atomic force microscope (AFM). The tip was a 0.01-0.025 Ω·cm antimony n-doped Si covered with conductive diamond. A 1000-4000 mV ac voltage was applied to the sample at 40 kHz using the VPFM mode. Surface photovoltage (SPV) measurements were performed with a halogen source with calibrated illumination with a single point Kelvin Probe system by KP Technology (KP020). The tip provided was in Au with a 2 mm diameter. For photovoltaic measurements, current-voltage (I-V) characteristics were carried out at room temperature using an Oriel VeraSol-2 AAA Solar Simulator in AM1.5G conditions and a Keithley 2461 SourceMeter. Contacts were made either directly with a tungsten tip on TMO or by depositing 1 mm² indium tin oxide (ITO) contacts.

3. Results and discussion

Because h-TMO films were found difficult to grow as the hexagonal phase is not the most favourable, we studied doping of TMO powders with different elements (M = In, Lu, Gd, Sm, Nd, Y) in order to stabilise the hexagonal phase against the orthorhombic one. The different compositions of $M_xTb_{1-x}MnO_3$ prepared are summarised in Table 1. For In, Lu and Y a value of x=0.20 was kept for comparison between the dopants. For Gd, Sm, Nd, because of the large size of the atoms, x was kept at 0.10. Figure 1 shows the XRD pattern of the different powders. It can be seen that for all the compositions shown, the characteristic peaks of o-TMO were preserved. In some cases, a parasitic phase of $TbMn_2O_5$ is observed in addition to the main o-TMO phase. For $In_{0.40}Tb_{0.60}MnO_3$ and $Lu_{0.40}Tb_{0.60}MnO_3$, the diffractogram did not match either o-TMO or h-TMO (see SI Figure S5). For all the other compositions, no sign of h-TMO could be detected but only o-TMO. Table 1 shows the lattice parameters extracted from Rietveld refinements, the volume V of the unit cell and the average atomic radius calculated as $V^{1/3}$. The ion-oxygen distance is indicated for each dopant element[22, 23]. First it can be seen that going from pure TMO to $In_{0.15}Tb_{0.85}MnO_3$ and $In_{0.20}Tb_{0.80}MnO_3$ the volume or average atomic radius is gradually decreasing. The effect looks much less pronounced with Lu, Gd, Sm, Y doping as $V^{1/3}$ stays in the 6.1 Å range. Nd doping shows a reduction of V and $V^{1/3}$ even more pronounced than for In in $In_{0.15}Tb_{0.85}MnO_3$. These results suggest than In and Nd are inserted in the TMO matrix while Lu, Gd, Sm, Y have low influence on the cell size. Two of the dopants were thus selected for fabrication of doped TMO targets, namely In, because of its large effect on V, and Y, because $YMnO_3$ is easily synthesized in the hexagonal phase[18] and is a known ferroelectric material[24]. Three aspects must be investigated with In-TMO and Y-TMO films, first the impact of the dopants on the formation of the hexagonal TMO phase, second the impact on the ferroelectric properties of the films and third the impact on the optical and photovoltaic properties.

Films of $TbMnO_3$ (TMO), $In_{0.20}Tb_{0.80}MnO_3$ (In-TMO), $Y_{0.20}Tb_{0.80}MnO_3$ (Y-TMO) and $YMnO_3$ (YMO) were then grown by PLD on Pt//ALO (0001). Pt is grown epitaxially by PLD and plays two key roles. The first one is that it is used as a conductive electrode for further ferroelectric and photovoltaic measurements. The second is that as shown in [18, 20, 25] the in-plane symmetry of the Pt layer is rotated by 30° in respect to the ALO (0001) substrate, leading to a Pt layer with hexagonal structure that is well adapted to h-TMO. Figure 2a shows the XRD pattern of the films grown at 10 Hz laser repetition rate and 2 J/cm² fluence. It can be seen that for all the films, Pt is grown epitaxially as demonstrated by the presence of the Pt (111) and (222) reflections. As opposed to o-TMO, h-TMO presents a distinct (0002) peak at around $2\theta=15.4°$[20]. It can be seen that the $YMnO_3$ is present only in the hexagonal phase, while for pure TMO and In-TMO both hexagonal and orthorhombic phases can be observed. Y-TMO does not show any distinct peak for the TMO phases. TMO films were grown at higher temperature (900 °C) at 10 Hz repetition rate and no improvement was observed.

Figure 2b shows the XRD pattern of films grown this time with 4 Hz repetition rate and 1 J/cm² fluence. Here, for pure TMO, In-TMO and Y-TMO only the hexagonal phase can be observed. This shows that by reducing the laser repetition rate and the laser fluence, thereby giving more time for growth kinetics after nucleation, the hexagonal phase can be obtained. The epitaxial relationship of the films is [1000]TMO(0001) / [2 -1 -1]Pt(111) // [2 1 -3 0]ALO(0001) as reported in [25]. Figure 2c shows a zoom in the 2θ region from 28 to 45°. It can be seen that while the Pt (111) and ALO (0006) are precisely in the same position, the position of the h-In-TMO (004) peak is noticeably shifted by about 0.2° to the left of the h-TMO (004) peak. The corresponding *c* lattice parameter is 11.463 Å for h-TMO and 11.531 Å for h-In-TMO. The former is an excellent match with previous values [25] and the latter means that *c* is increased by 0.6 % with In doping which is a sign that In is inserted in the h-TMO matrix as it was the case for the o-TMO powders.

The optical properties of the films were investigated by spectroscopic ellipsometry as discussed in the experimental section. As a matter of fact, calculations for pure h-TMO in [12] indicate extraordinary optical linear dichroism and linear birefringence properties. Figure 3a shows the ordinary α_o (light polarization in the ab plane) and extraordinary α_e (light polarization along the c axis) absorption coefficients for h-TMO, h-In-TMO, h-Y-TMO films and for the h-TMO calculation[12]. It can be observed that between experimental and calculated h-TMO absorption coefficients the absorption band edge is less than 0.4 eV apart so that globally the match is globally satisfactory. It is well known that calculations cannot predict precisely the bandgap of materials. Only the complex shape above 2 eV for the ordinary contribution is not visible in the experimental data. The predicted high α_o absorption plateau of around 10^5 cm^{-1} is also present. The doped h-TMO films provide similar properties to pure h-TMO, apart from the extraordinary contribution of h-In-TMO that has a band edge 0.6 eV higher. In-doping causes a stronger modification of lattice parameters than Y-doping, as evidenced in Figure 2c. It was also the case for o-TMO as shown in Table 1. Lattice parameters changes are well known to modify the bandgap properties [26] and therefore the absorption coefficients. The Tauc plots extracted from α_o are shown in Figure 3b. A direct bandgap of 1.55, 1.61 and 1.60 eV is observed for h-TMO, h-In-TMO and h-Y-TMO respectively, which is a good match with previously reported values[27]. The high absorption coefficient 10^5 cm^{-1}, the values of the bandgap of about 1.6 eV, and the low thicknesses of the films can be compared to similar values for another material in the two dimensional form, MoSSe, that is envisaged as a water-splitting photocatalyst [28, 29].

In the next part, we report on the electrical properties of the PLD films. PFM was performed to investigate the possible ferroelectricity of the films. It was found that the h-TMO, h-In-TMO and h-Y-TMO did not provide any clear ferroelectric loop with a well-defined hysteresis nor poling images indicating ferroelectricity. Only the h-YMO film showed ferroelectric characteristics, as shown in Figure

4, but with a very low hysteresis voltage (see SI Figure S6 for the other samples). The first report on ferroelectricity in h-TMO by Lee et al. found a Curie temperature well below room temperature, around 60 K, based on dielectric and electrical measurements[25]. Eight years later Kim et al. performed PFM on h-TMO at room temperature and by heating up to 180 °C, while hysteretic PFM loops were observed[18]. In the present case we do not observe any sign of ferroelectricity at room temperature, except for h-YMO. The surface of the films was found very flat with root-mean-square (RMS) roughness below 0.6 nm over 0.25 µm² (see SI Figure S7).

I-V characteristics under 1 sun showed that the short-circuit current I_{SC} of the structures was below the detection limit of the equipment (below 0.1 nA). The I-V characteristics were not showing any rectification but rather a tunnelling behaviour. This indicates that the films are extremely resistive which may account for the absence of a short-circuit current I_{SC}. Voltage pulses up to ±10 V did not provide any change on the I_{SC}.

Another powerful technique that was used to investigate the photovoltaic properties is the surface photovoltage (SPV). It is based on a Kelvin probe setup where the sample is illuminated with a white light while monitoring the contact potential difference (CPD). Figure 5a shows such a measurement for the different devices. The Pt electrode is connected to the ground while an Au tip is approached to the surface of the manganite films. The h-TMO and In-TMO show no response to light, while h-Y-TMO shows a better response than h-YMO. This means that both h-Y-TMO and h-YMO provide a photovoltaic response. The SPV signal determined as SPV = CPD(light)-CPD(dark) is shown in Figure 5b as a function of illumination of the halogen light source and confirms the observation of the photovoltaic behaviour. In this solar cell configuration, the SPV signal is related to the open-circuit voltage which is found to be the highest for the h-Y-TMO sample with about 80 mV at 20 mW/cm². This corresponds to a relatively large area measurement as the tip has a 2 mm diameter. Therefore it is clear that doping has a large impact on the photovoltaic properties of h-TMO and that the properties of h-YMO can be surpassed with h-Y-TMO which may encourage further research.

4. Conclusions

Powders of doped TMO were investigated to encourage the formation of an hexagonal TMO phase. In and Nd incorporation were found to greatly reduce the TMO cell size without leading to a hexagonal phase. Hexagonal films of TMO, In-TMO, Y-TMO and YMO were obtained thanks to epitaxial stabilisation on Pt (111), by carefully adjusting the PLD laser repetition rate to 4 Hz. The optical properties namely the absorption coefficient and the bandgap were determined for TMO, In-TMO, and

Y-TMO films. Birefringence was found in these films. The absorption coefficient was about 10^5 cm^{-1} at 2 eV for the TMO and doped TMO films and the direct bandgap in the 1.5-1.6 eV range (ordinary contribution). Concerning the ferroelectric properties of the films at room temperature, only the h-YMO films showed a ferroelectric-like hysteretic behaviour by PFM. I-V measurements under 1 sun showed the absence of any measurable and switchable I_{SC}. Tunnelling-like I-V curves were obtained and the high resistivity observed may account for the low I_{SC} observed. Still, the h-Y-TMO and h-YMO films provide a photovoltaic response as observed by SPV which is a sign that incorporation of Y has a beneficial effect on the PV properties. Further work on h-TMO for PV and photoferroelectric applications should focus on the increase of conductivity of the materials for example with additional dopants.

Declaration of Competing Interest

The authors declare that they have no known competing financial interests or personal relationships that could have appeared to influence the work reported in this paper.

Acknowledgments

The authors thank the XRD and SEM platforms of IPCMS including M. Lenertz and C. Leuvrey, and the staff of the C^3Fab platform of ICube. This work was partly carried out under the framework of the FERROPV project supported by the French Agence Nationale de la Recherche (ANR) under the reference ANR-16-CE050002-01.

Table 1: a,b,c lattice parameters obtained from Rietveld refinement for the different powders synthesised and from the ICDD TMO reference. The volume of the cell, the average atomic radius and the ion-oxygen distance from [22, 23] [23] are also indicated. The error bar on a,b,c is ± 0.005 Å**.**

Formula	**a (Å)**	**b (Å)**	**c (Å)**	**Volume ($Å^3$)**	**Average atomic radius $V^{1/3}$ (Å)**	**Ion-oxygen distance (Å)**
$TbMnO_3$ ICDD 025-0933	5.294	5.839	7.399	228.7	6.115	2.618 (Tb^{3+})
$TbMnO_3$ as fabricated	5.308	5.803	7.413	228.3	6.112	2.618 (Tb^{3+})
$In_{0.15}Tb_{0.85}MnO_3$	5.295	5.789	7.378	226.2	6.093	2.520 (In^{3+})
$In_{0.20}Tb_{0.80}MnO_3$	5.267	5.631	7.324	217.2	6.011	2.520 (In^{3+})
$Lu_{0.20}Tb_{0.80}MnO_3$	5.322	5.800	7.387	228.0	6.109	2.559 (Lu^{3+})
$Gd_{0.10}Tb_{0.90}MnO_3$	5.316	5.798	7.363	227.0	6.100	2.628 (Gd^{3+})
$Sm_{0.10}Tb_{0.90}MnO_3$	5.302	5.796	7.401	227.4	6.104	2.648 (Sm^{3+})
$Nd_{0.10}Tb_{0.90}MnO_3$	5.300	5.789	7.334	225.0	6.083	2.667 (Nd^{3+})
$Y_{0.20}Tb_{0.80}MnO_3$	5.307	5.799	7.426	228.5	6.114	2.596 (Y^{3+})

Figure 1: Room temperature θ-2θ XRD pattern showing the different powders measured and the ICDD references.

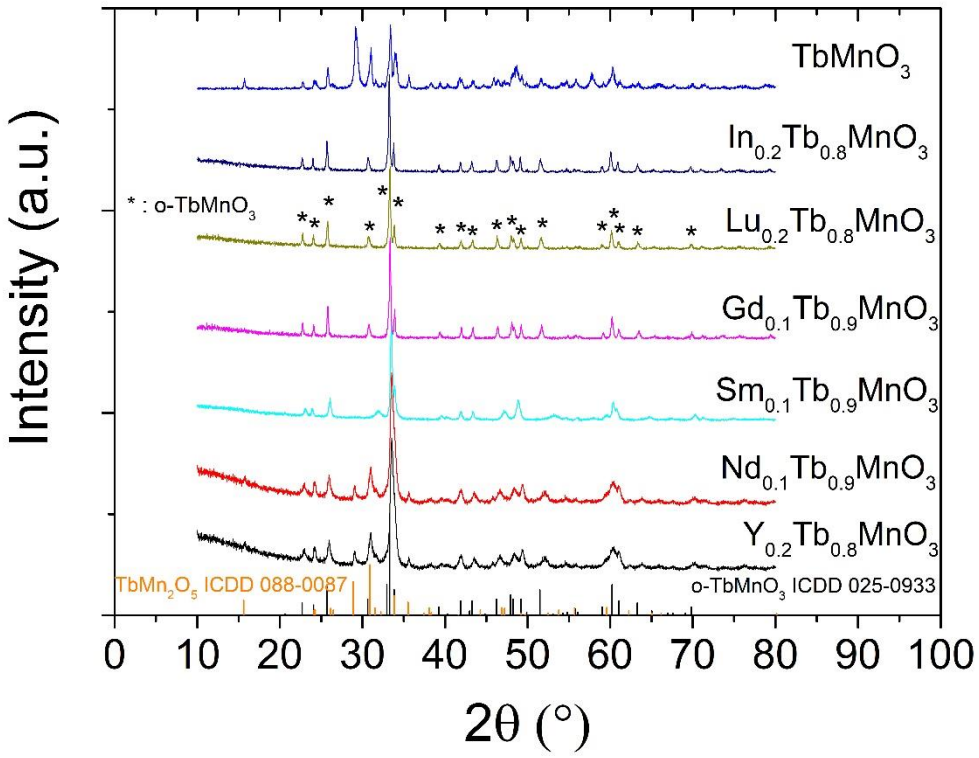

Figure 2: Room temperature θ-2θ XRD patterns showing the different films grown on Pt//Al_2O_3 (0001) at a) 10 Hz b) 4Hz laser repetition rate during PLD growth and c) is a zoom of b).

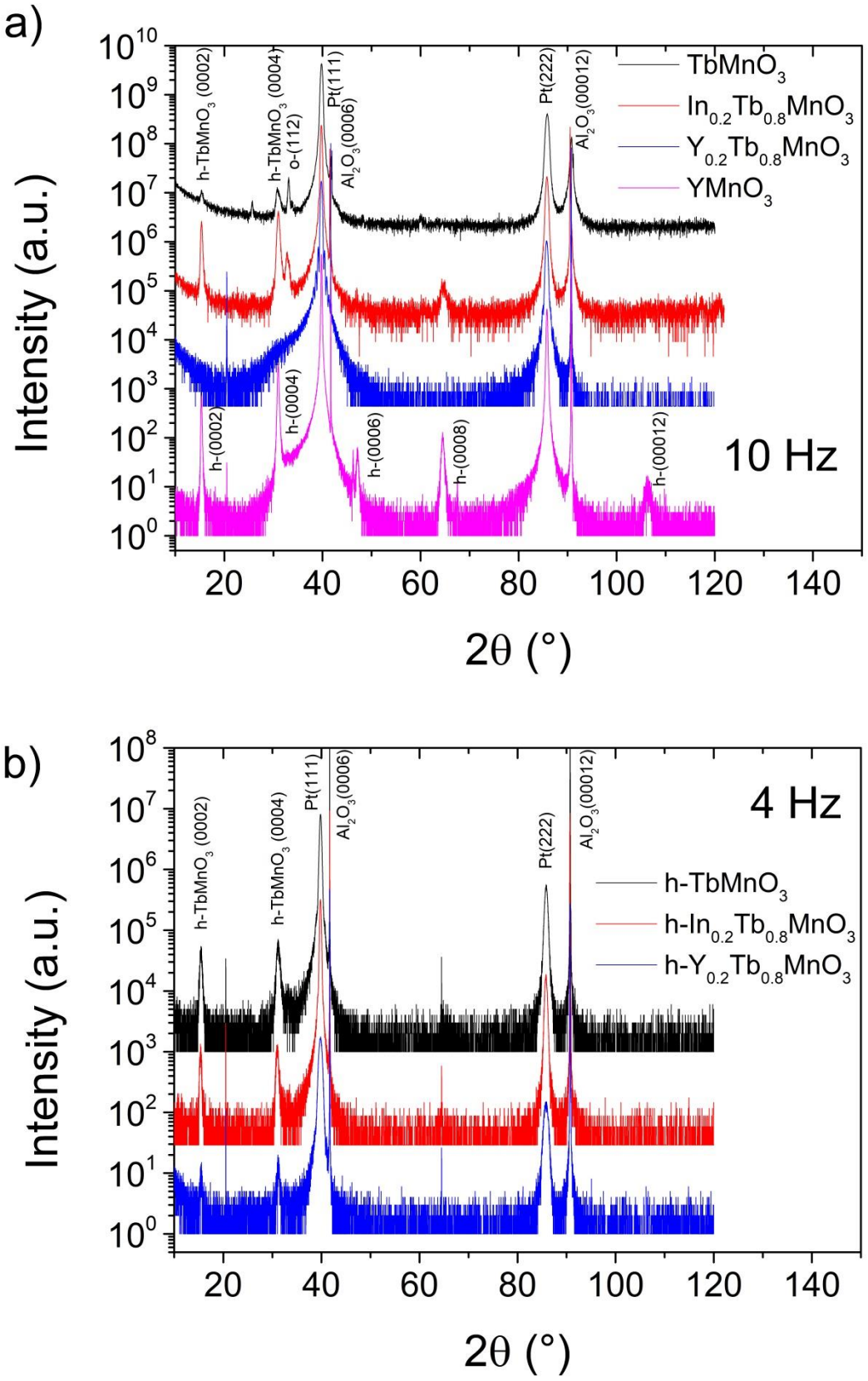

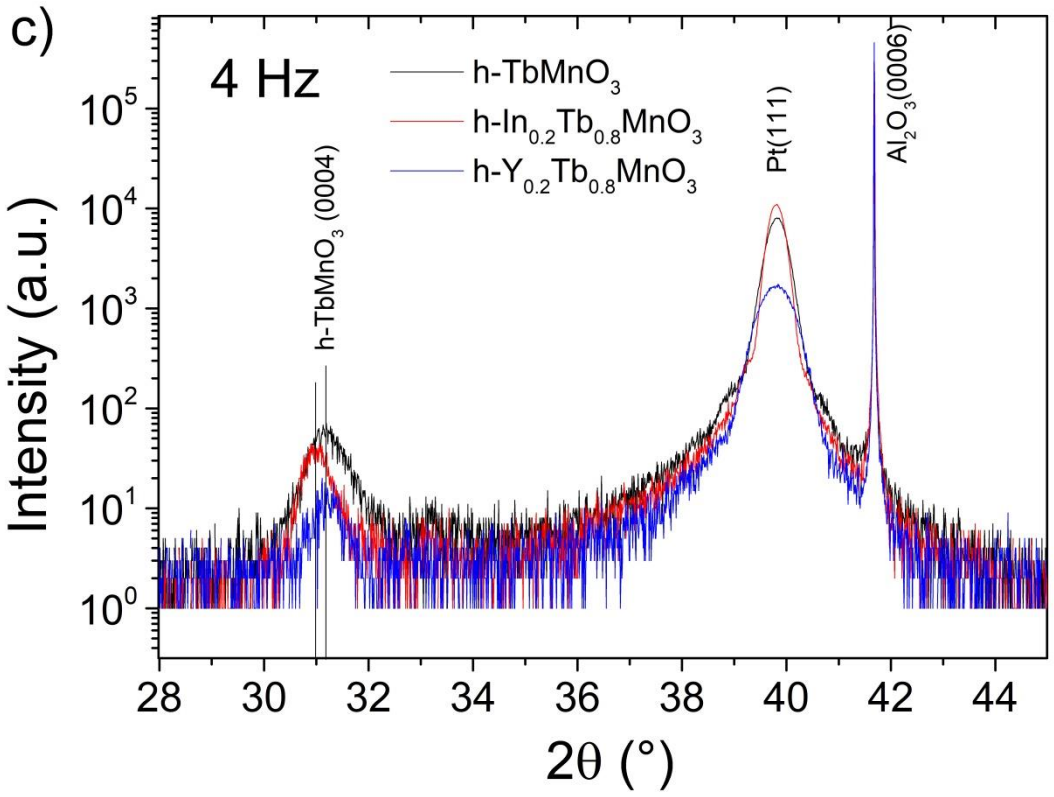
c)
4 Hz
h-TbMnO3
h-In0.2Tb0.8MnO3
h-Y0.2Tb0.8MnO3
h-TbMnO3 (0004)
Pt(111)
Al2O3(0006)
Intensity (a.u.)
2θ (°)

Figure 3: a) Absorption coefficient vs. photon energy for the different layers as calculated from spectroscopic ellipsometry. b) Corresponding Tauc's plot assuming a direct bandgap.

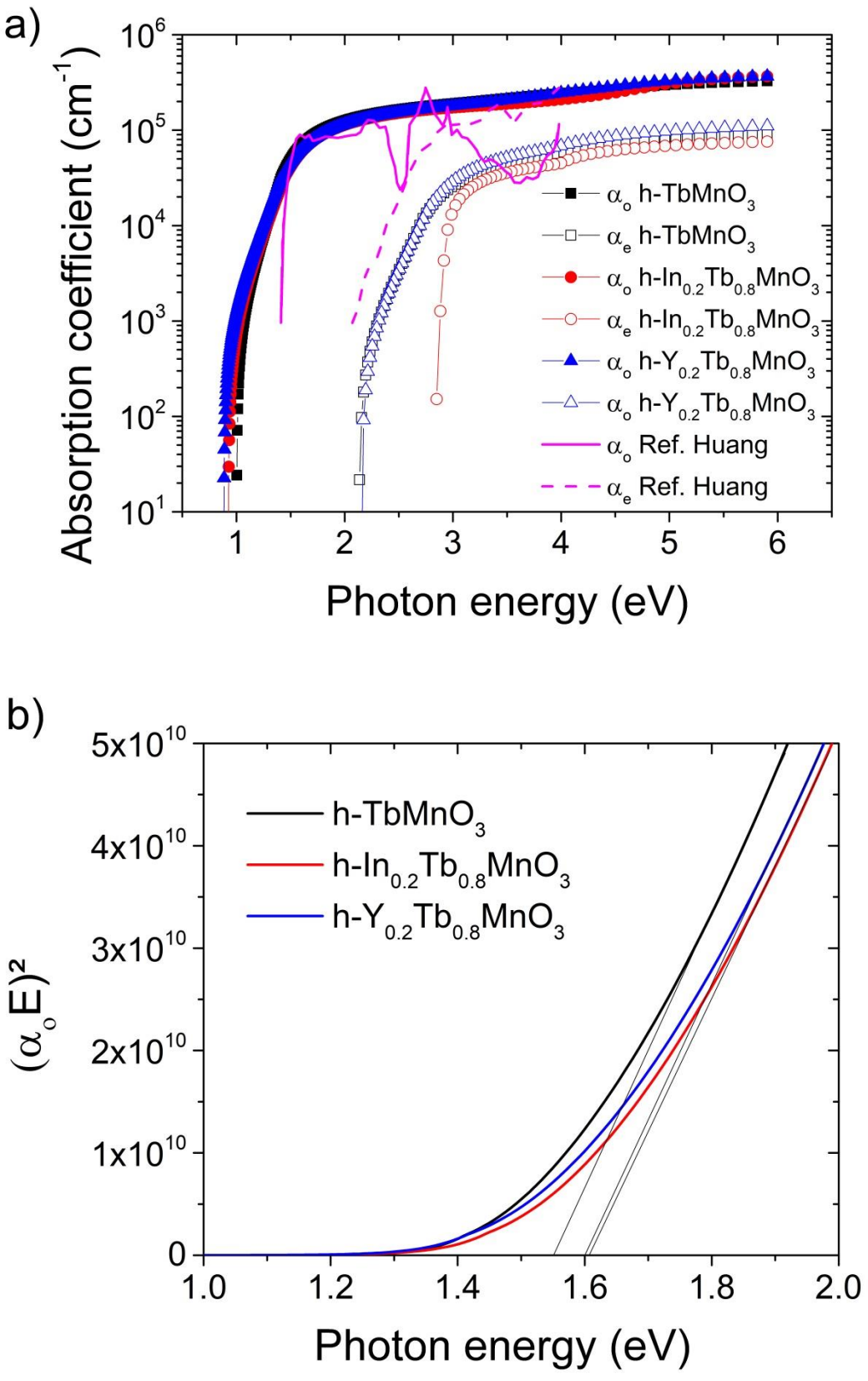

Figure 4: PFM phase and amplitude hysteresis loops at room temperature as a function of the tip bias voltage for a) h-$TbMnO_3$ and b) h-$YMnO_3$ films.

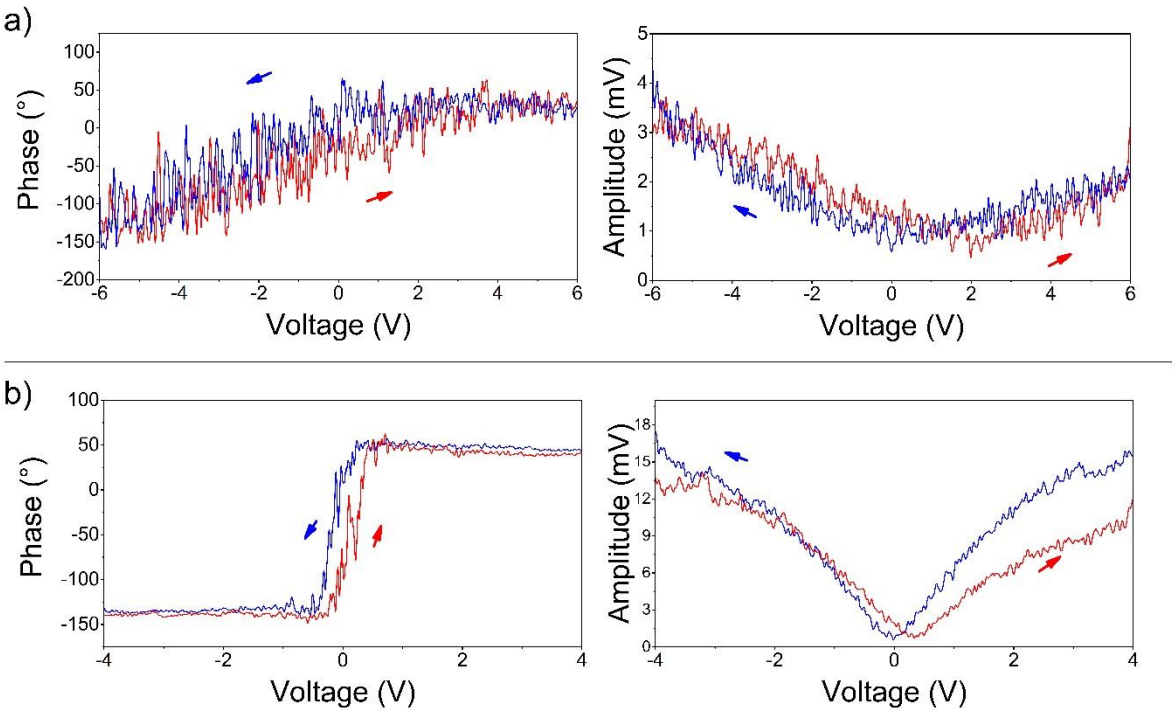

Figure 5: a) Contact potential difference (CPD) from the Kelvin probe as a function of time alternating between dark and halogen visible light. b) Surface photovoltage (SPV) from the Kelvin probe under variable halogen visible light illumination.

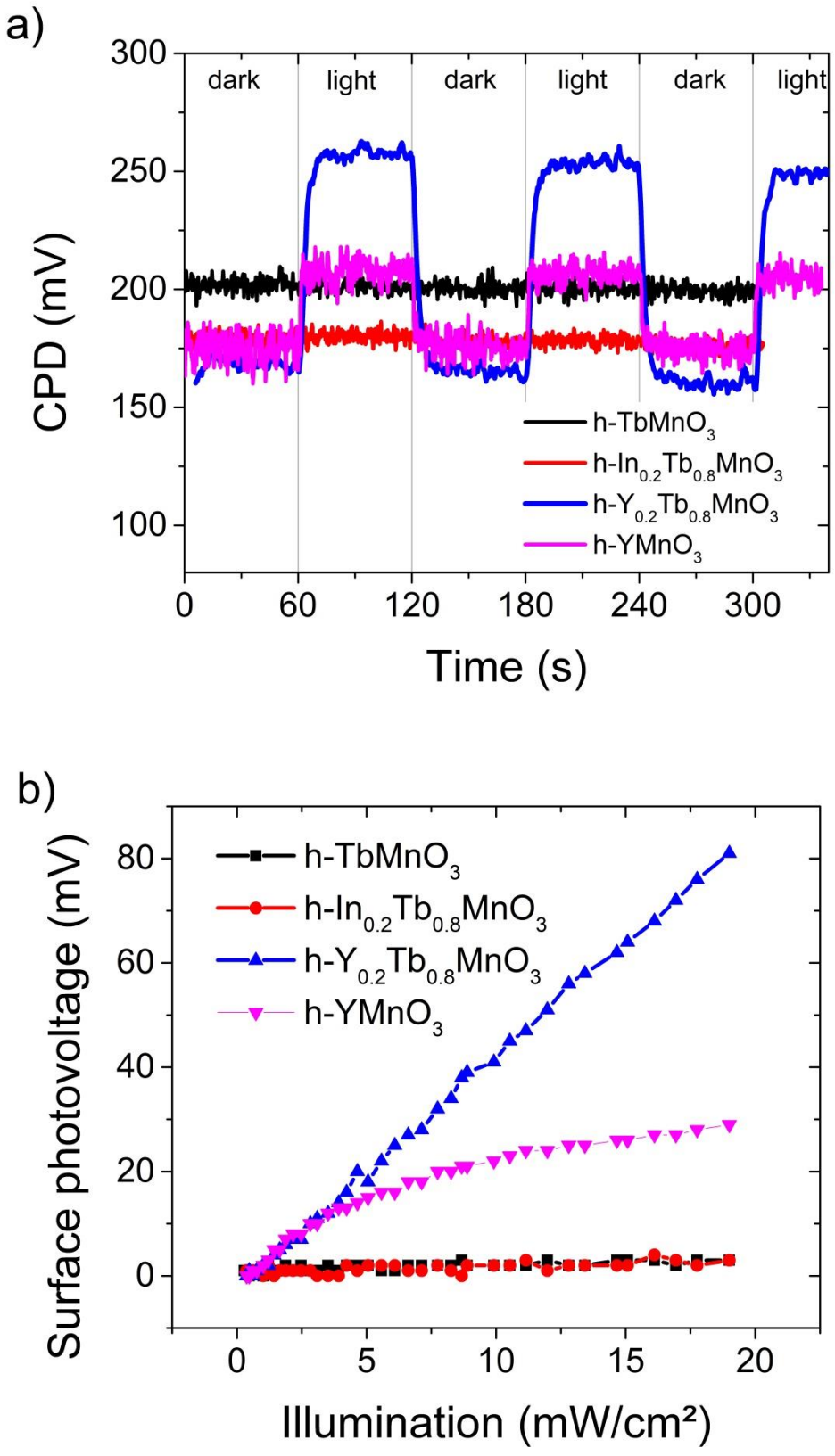

References

[1] S.Y. Yang, J. Seidel, S.J. Byrnes, P. Shafer, C.H. Yang, M.D. Rossell, P. Yu, Y.H. Chu, J.F. Scott, J.W. Ager, L.W. Martin, R. Ramesh, Above-bandgap voltages from ferroelectric photovoltaic devices, Nature Nanotechnology, 5 (2010) 143-147. https://doi.org/10.1038/nnano.2009.451

[2] R. Nechache, C. Harnagea, S. Li, L. Cardenas, W. Huang, J. Chakrabartty, F. Rosei, Bandgap tuning of multiferroic oxide solar cells, Nature Photonics, 9 (2015) 61-67. https://doi.org/10.1038/nphoton.2014.255

[3] M. Alexe, D. Hesse, Tip-enhanced photovoltaic effects in bismuth ferrite, Nat. Commun., 2 (2011) 256. https://doi.org/10.1038/ncomms1261

[4] J. Belhadi, J. Ruvalcaba, S. Yousfi, M. El Marssi, T. Cordova, S. Matzen, P. Lecoeur, H. Bouyanfif, Conduction mechanism and switchable photovoltaic effect in (111) oriented BiFe0.95Mn0.05O3 thin film, J. Phys.-Condes. Matter, 31 (2019) 7. https://doi.org/10.1088/1361-648X/ab157e

[5] A. Quattropani, D. Stoeffler, T. Fix, G. Schmerber, M. Lenertz, G. Versini, J.L. Rehspringer, A. Slaoui, A. Dinia, S. Cois, Band-Gap Tuning in Ferroelectric Bi2FeCrO6 Double Perovskite Thin Films, Journal of Physical Chemistry C, 122 (2018) 1070-1077. https://doi.org/10.1021/acs.jpcc.7b10622

[6] A. Quattropani, A.S. Makhort, M.V. Rastei, G. Versini, G. Schmerber, S. Barre, A. Dinia, A. Slaoui, J.L. Rehspringer, T. Fix, S. Colis, B. Kundys, Tuning photovoltaic response in Bi2FeCrO6 films by ferroelectric poling, Nanoscale, 10 (2018) 13761-13766. https://doi.org/10.1039/c8nr03137a

[7] T. Fix, G. Schmerber, H. Wang, J.L. Rehspringer, C. Leuvrey, S. Roques, M. Lenertz, D. Muller, H. Wang, A. Slaoui, Investigation of KBiFe2O5 as a Photovoltaic Absorber, Acs Applied Energy Materials, 2 (2019) 8039-8044. https://doi.org/10.1021/acsaem.9b01509

[8] T. Fix, Oxide and Ferroelectric Solar Cells, in: D.G.a.T. Fix (Ed.) Advanced Micro- and Nanomaterials for Photovoltaics, Elsevier, 2019, pp. 19-34.

[9] A.M. A. Pérez-Tomás, D. Tanenbaum and M. Lira-Cantú, Metal Oxides in Photovoltaics: All-Oxide, Ferroic, and Perovskite Solar Cells, in: M. Lira-Cantú (Ed.) The Future of Semiconductor Oxides in Next-Generation Solar Cells, Elsevier, 2018, pp. 267-356.

[10] H. Han, S. Song, J.H. Lee, K.J. Kim, G.W. Kim, T. Park, H.M. Jang, Switchable Photovoltaic Effects in Hexagonal Manganite Thin Films Having Narrow Band Gaps, Chem. Mat., 27 (2015) 7425-7432. https://doi.org/10.1021/acs.chemmater.5b03408

[11] H. Han, D. Kim, S. Chae, J. Park, S.Y. Nam, M. Choi, K. Yong, H.J. Kim, J. Son, H.M. Jang, Switchable ferroelectric photovoltaic effects in epitaxial h-RFeO3 thin films, Nanoscale, 10 (2018) 13261-13269. https://doi.org/10.1039/c7nr08666k

[12] X. Huang, T.R. Paudel, S. Dong, E.Y. Tsymbal, Hexagonal rare-earth manganites as promising photovoltaics and light polarizers, Phys. Rev. B, 92 (2015) 8. https://doi.org/10.1103/PhysRevB.92.125201

[13] M.L. Li, H.X. Tan, W.H. Duan, Hexagonal rare-earth manganites and ferrites: a review of improper ferroelectricity, magnetoelectric coupling, and unusual domain walls, Phys. Chem. Chem. Phys., 22 (2020) 14415-14432. https://doi.org/10.1039/d0cp02195d

[14] T. Kimura, T. Goto, H. Shintani, K. Ishizaka, T. Arima, Y. Tokura, Magnetic control of ferroelectric polarization, Nature, 426 (2003) 55-58. https://doi.org/10.1038/nature02018

[15] K. Shimamoto, S. Mukherjee, S. Manz, J.S. White, M. Trassin, M. Kenzelmann, L. Chapon, T. Lippert, M. Fiebig, C.W. Schneider, C. Niedermayer, Tuning the multiferroic mechanisms of TbMnO3 by epitaxial strain, Sci Rep, 7 (2017) 9. https://doi.org/10.1038/srep44753

[16] A. Glavic, J. Voigt, J. Persson, Y.X. Su, J. Schubert, J. de Groot, W. Zande, T. Bruckel, High quality TbMnO3 films deposited on YAlO3, Journal of Alloys and Compounds, 509 (2011) 5061-5063. https://doi.org/10.1016/j.jallcom.2011.03.015

[17] K.X. Jin, Y.X. Zhai, H. Li, Y.F. Tian, B.C. Luo, T. Wu, Favorable ultraviolet photoelectric effects in TbMnO3/Nb-SrTiO3 heterostructures, Solid State Commun., 199 (2014) 39-42. https://doi.org/10.1016/j.ssc.2014.09.004

[18] D.J. Kim, T.R. Paudel, H.D. Lu, J.D. Burton, J.G. Connell, E.Y. Tsymbal, S.S.A. Seo, A. Gruverman, Room-Temperature Ferroelectricity in Hexagonal TbMnO3 Thin Films, Adv. Mater., 26 (2014) 7660-7665. https://doi.org/10.1002/adma.201403301
[19] R. Mandal, M. Hirsbrunner, V. Roddatis, R. Gruhl, L. Schuler, U. Ross, S. Merten, P. Gegenwart, V. Moshnyaga, Strain-driven structure-ferroelectricity relationship in hexagonal TbMnO3 films, Phys. Rev. B, 102 (2020) 10. https://doi.org/10.1103/PhysRevB.102.104106
[20] J.H. Lee, D. Lee, T.W. Noh, P. Murugavel, J.W. Kim, K.H. Kim, Y. Jo, M.H. Jung, J.G. Yoon, J.S. Chung, Formation of hexagonal phase of TbMnO3 thin film and its multiferroic properties, J. Mater. Res., 22 (2007) 2156-2162. https://doi.org/10.1557/jmr.2007.0270
[21] H. Yoshikawa, S. Adachi, Optical constants of ZnO, Jpn. J. Appl. Phys., Part 1, 36 (1997) 6237-6243. https://doi.org/10.1143/jjap.36.6237
[22] P. Poix, Ann. Chim., 9 (1964) 261.
[23] P. Poix, Ann. Chim., 10 (1965) 49.
[24] H.Z. Pang, F.Y. Zhang, M. Zeng, X.S. Gao, M.H. Qin, X.B. Lu, J.W. Gao, J.Y. Dai, Q.L. Li, Preparation of epitaxial hexagonal YMnO3 thin films and observation of ferroelectric vortex domains, npj Quantum Mater., 1 (2016) 16015. https://doi.org/10.1038/npjquantmats.2016.15
[25] J.H. Lee, P. Murugavel, H. Ryu, D. Lee, J.Y. Jo, J.W. Kim, H.J. Kim, K.H. Kim, Y. Jo, M.H. Jung, Y.H. Oh, Y.W. Kim, J.G. Yoon, J.S. Chung, T.W. Noh, Epitaxial stabilization of a new multiferroic hexagonal phase of TbMnO3 thin films, Advanced Materials, 18 (2006) 3125-+. https://doi.org/10.1002/adma.200601621
[26] T. Fix, D. Stoeffler, S. Colis, C. Ulhaq, G. Versini, J.P. Vola, F. Huber, A. Dinia, Effects of strain relaxation on the electronic properties of epitaxial Sr2FeMoO6 grown by pulsed laser deposition on SrTiO3 (001), Journal of Applied Physics, 98 (2005) 4. https://doi.org/10.1063/1.1925761
[27] W.S. Choi, D.G. Kim, S.S.A. Seo, S.J. Moon, D. Lee, J.H. Lee, H.S. Lee, D.Y. Cho, Y.S. Lee, P. Murugavel, J. Yu, T.W. Noh, Electronic structures of hexagonal RMnO3 (R=Gd, Tb, Dy, and Ho) thin films: Optical spectroscopy and first-principles calculations, Phys. Rev. B, 77 (2008) 045137. https://doi.org/10.1103/PhysRevB.77.045137
[28] X.C. Ma, X. Wu, H.D. Wang, Y.C. Wang, A Janus MoSSe monolayer: a potential wide solar-spectrum water-splitting photocatalyst with a low carrier recombination rate, Journal of Materials Chemistry A, 6 (2018) 2295-2301. https://doi.org/10.1039/c7ta10015a
[29] X.C. Ma, X. Yong, C.C. Jian, J.Q. Zhang, Transition Metal-Functionalized Janus MoSSe Monolayer: A Magnetic and Efficient Single-Atom Photocatalyst for Water Splitting Applications, Journal of Physical Chemistry C, 123 (2019) 18347-18354. https://doi.org/10.1021/acs.jpcc.9b03003